Optimization of vortex pinning by nanoparticles using simulations of the time-dependent Ginzburg-Landau model

A. E. Koshelev, I. A. Sadovskyy, C. L. Phillips, and A. Glatz

Phys. Rev. B **93**, 060508 — Published 29 February 2016

DOI: 10.1103/PhysRevB.93.060508

Optimization of vortex pinning by nanoparticles using simulations of time-dependent Ginzburg-Landau model

A. E. Koshelev,[1] I. A. Sadovskyy,[1] C. L. Phillips,[2] and A. Glatz[1,3]

[1] *Materials Science Division, Argonne National Laboratory, 9700 S. Cass Av., Argonne, Il 60639, USA*
[2] *Mathematics and Computer Science Division, Argonne National Laboratory, 9700 S. Cass Av., Argonne, Il 60639, USA*
[3] *Department of Physics, Northern Illinois University, DeKalb, Il 60115, USA*

(Dated: February 8, 2016)

Incorporating nanoparticles into superconducting materials has emerged as an efficient route to enhance their current-carrying capability. However, a thorough understanding of how these inclusions can be used in the most efficient way is still lacking. We address this problem of optimizing the vortex pinning landscape for randomly distributed metallic spherical inclusions using systematic large-scale numerical simulations of time-dependent Ginzburg-Landau equations. This approach allows us to predict the size and density of particles for which the highest critical current is realized. For a given particle size and magnetic field, the critical current reaches a maximum value at a particle density, which typically corresponds to 15–23% of the total volume being replaced by the nonsuperconducting material. For a fixed diameter, this optimal particle density increases with the magnetic field. Moreover, we found that, as the magnetic field increased, the optimal particle diameter slowly decreases from 4.5 to 2.5 coherence lengths. This result shows that pinning landscapes have to be designed for specific applications taking into account relevant magnetic field scales.

PACS numbers: 74.20.De, 74.25.Sv, 74.25.Wx

Pinning of vortex lines by defects is essential for superconductor's ability to carry electrical current without dissipation. Thus, high-current applications of superconductivity require engineering defect microstructures to efficiently suppress the mobility of vortices over a wide range of magnetic fields. On the other hand, vortex matter in disordered superconductors represents a complex system with extremely rich and non-trivial dynamics that has challenged researchers for more than five decades. As this field is of high fundamental and practical importance, great efforts have been devoted in the past to establishing basic laws of pinning [1–3]. Two most studied limiting cases are a very high density of weak centers described by the collective pinning theory [4], and a low density of large-size pins, described by the strong-pinning theory [5, 6]. In addition to analytical theories, pinning has also been extensively explored by Langevin-dynamics simulations for both isolated elastic string [7, 8], and array of interacting strings [9–12].

Interest in the strong-pinning scenario has been renewed recently due to its relevance for $YBa_2Cu_3O_7$ (YBCO) films with self-assembled inclusions which strongly enhance critical currents in these films. Such inclusions may be prepared in the form of almost spherical particles [13–19], nanorods [20], or combinations of both [21]. This technology has been implemented in the second-generation superconducting cables based on YBCO coated conductors [22] operating in a wide range of magnetic fields. In addition to self-assembly, large-size defects in the form of impurity clusters can also be introduced by proton irradiation [23, 24].

Increased ability to engineer a pinning microstructures raises the following question: At what sizes and densities of inclusions does the critical current reach its maximum for different magnetic field and temperatures. This fundamental problem of pinning optimization cannot be resolved by simple approaches. Indeed, both analytical theory [5, 6] and Langevin-dynamics simulations [7–12] can evaluate the critical current only in the case when particles occupy small fraction of the material. While the ultimate critical-current optimization can be achieved by the constructive combination of different pinning centers, a natural first step is to determine the best pinning configuration for a relatively simple system with only one type of defects. In this Letter, we explore the case of monodisperse spherical defects with diameters of a few coherence lengths using large-scale simulations of the time-dependent Ginzburg-Landau (TDGL) model [25], allowing for a systematic study of arbitrary defect concentrations, while at the same time taking the collective behavior and the intricate intrinsic interactions of the vortex matter into account.

The TDGL model describes dynamics of the superconducting order parameter and the vortex lines appear spontaneously as its singularities. Even though the TDGL model does not provide a fully realistic description of the dynamic properties of superconductors, it does describe accurately vortex-line flexibility, interactions between vortex lines, and interactions of vortices with pinning sites. It also allows for cuttings and reconnections of vortex lines. Therefore, this model is perfectly suited for the problem of the critical-current optimization, for which a fully accurate description of the dynamics is not essential. The TDGL model has been proven to be very useful for exploring many properties of the vortex state [26–34]. However, only recently a mean-

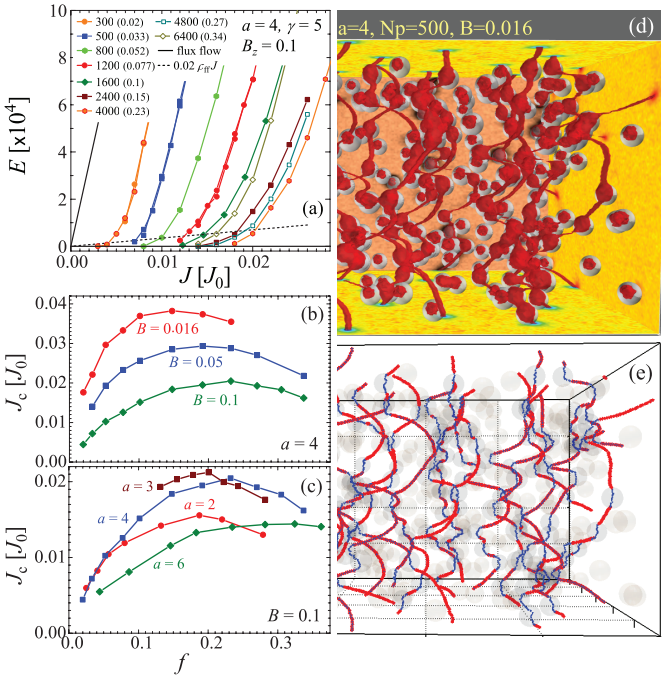

Figure 1. (a) Current-voltage dependences computed for different numbers of particles N_p with diameter $a = 4\xi$ for magnetic field $0.1H_{\mathrm{C2}}$. The numbers in parentheses represent the volume fractions occupied by the particles f. The critical currents are determined by the intersection of the CVD and 2% of the flux flow voltage (dashed line). The optimal concentration of particles is at $N_\mathrm{p} = 4\,000$ corresponding to $f = 0.23$. (b) The dependences of the critical current J_C on the particle volume fraction f for $a = 4\xi$ and three magnetic fields. The optimal f increases with the magnetic field. (c) The dependences of J_C on f for different particle diameters at $B = 0.1H_{\mathrm{C2}}$. The optimal particle diameter is in between 3ξ and 4ξ. (d) Order parameter isosurfaces for a pinned vortex configurations with $a = 4\xi$, $N_\mathrm{p} = 500$, and $B = 0.016H_{\mathrm{C2}}$. (e) The field-induced vortex lines extracted from the same order parameter. The particles are shown as transparent spheres. Vortex lines outside particles are red, and inside particles are blue.

ingful exploration of the parameter space for sufficiently large three-dimensional superconductor has became possible [35] allowing us to address the problem of critical-current optimization.

We use the TDGL model to explore vortex pinning by randomly-placed metallic spherical inclusions. Our objective is to find the optimal parameters for the pinning landscape to maximize the critical current. Clearly, when the particles occupy a small fraction of the total volume, the critical current grows as particle density increases. At some density, however, further increase of particle number will not improve current-carrying capacity [36] due to at least two factors: (i) The increasing mobility of the vortex lines due to jumping between the particles and (ii) the reduction the effective cross section for the supercurrent caused by inclusions. Therefore, it is important to find the size and density of particles that maximizes the critical current. This problem can not be accessed by simple approaches. We find optimal parameters for different magnetic fields by systematically exploring the dependence of the critical current on size and concentration of particles.

The dynamics of the order parameter $\psi(\mathbf{r},t)$ is described by the TDGL equation in the reduced form

$$(\partial_t + \imath\mu)\psi = \epsilon(\mathbf{r})\psi - |\psi|^2\psi + \sum_{j=x,y,z} \eta_j^2(\nabla_j - \imath A_j)^2\psi + \zeta(\mathbf{r},t). \quad (1)$$

Here μ and $\mathbf{A}$ are the scalar and vector potentials. We used the in-plane coherence length ξ at the chosen temperature as the unit of length, meaning that $\eta_x = \eta_y = 1$ and $\eta_z = 1/\gamma$, were γ is the anisotropy factor. We took $\gamma = 5$ corresponding to YBCO. The function $\epsilon(\mathbf{r})$ models pinning centers, $\epsilon(\mathbf{r}) = 1$ in the bulk [37] and $\epsilon(\mathbf{r}) = -1$ inside metallic inclusions. We used the approximation of large London penetration depth λ in which the vector potential $\mathbf{A}$ is fixed by the external magnetic field, $A_y = Bx$, and the magnetic field is measured in units of the c-axis upper critical field at given temperature, $H_{\mathrm{C2}} = \Phi_0/2\pi\xi^2$. The Langevin term $\zeta(\mathbf{r},t)$ describing thermal noise has the correlation function $\langle\zeta^*(\mathbf{r},t)\zeta(\mathbf{r}',t')\rangle = T\,\delta(\mathbf{r}-\mathbf{r}')\,\delta(t-t')$, where T is the reduced temperature in units of $H_\mathrm{C}^2\xi^3/8\pi$ and H_C is the thermodynamic field. The total electric current in units of $J_0 = c\Phi_0/8\pi^2\xi\lambda^2$ (CGS) is given by

$$J_j = \eta_j^2\left(\mathrm{Im}[\psi^*(\nabla_j - \imath A_j)\psi] - \nabla_j\mu\right), \quad (2)$$

where the first term is the supercurrent and the second term gives the normal current. In these units the depairing current is $J_\mathrm{dp} = 2/3\sqrt{3}J_0 \approx 0.385J_0$. We performed simulations with fixed current applied in the x direction and compute the average electric field $E = -\nabla_x\mu$ in the dynamic steady state. For the simulations, we developed a stable and efficient solver implemented for graphics processing units [35]. The simulated system size is $100\xi \times 100\xi \times 50\xi$ with $256 \times 256 \times 128$ mesh points and we used periodic boundary conditions in all directions [38]. The external current is applied along the x axis. The procedure for fixing the current density flowing through the system is described in Ref. [35]. We fixed the reduced temperature at very small value $T = 4\times10^{-5}$ corresponding to real temperature $\lesssim 1\,\mathrm{K}$ meaning that thermal noise is not essential in these simulations. The time discretization step is selected to be 0.1 in units of the Ginzburg-Landau time.

We systematically computed the current-voltage dependences (CVDs) for different particle sizes and densities. Figure 1(a) shows representative series of CVDs for different numbers of particles N_p with diameter of $a = 4\xi$ at magnetic field $B = 0.1H_{\mathrm{C2}}$ corresponding to 159 vortex lines in the system. These CVDs are obtained

by stepwise decrease of the applied current with a simulation time of about 10^5 units of the Ginzburg-Landau time between current steps. Typically, we did not observe significant history effects: CVDs computed with different starting currents and current steps are found to be very similar to each other. Only at small magnetic fields $\sim 0.01H_{c2}$ CVDs become more noisy and slightly history-dependent.

The pinning effectiveness of the particles is primarily determined by the volume fraction f occupied by them. For spatially separated particles the "nominal" volume fraction is $f_n = \pi N_p a^3/6L_xL_yL_z$. As in our case randomly-placed particles may overlap, the real volume fraction is somewhat smaller, $f \approx f_n - f_n^2/2$, where the correction term accounts for possible overlaps between pairs of neighboring spheres. For each number of particles, the value of f is specified in parenthesis in Fig. 1(a). For low f the CVDs systematically shift to the right as particle density increases indicating an increase of the critical current. Above a certain density adding more particles starts to degrade the critical current. The optimal density corresponds to the volume fraction $f = 0.23$.

The computed CVDs are used to evaluate the critical currents, J_c, which we define using the criterion $E(J_c) = 0.02\rho_{ff}J_c$ [dashed line in Fig. 1(a)]. The free flux-flow resistivity, ρ_{ff}, in our reduced units is $\rho_{ff} = 1.689B$. Figure 1(b) shows the dependences of the critical current on the nonsuperconducting volume fraction f for $a = 4\xi$ and three magnetic fields. The optimal volume fraction slowly increases with the magnetic field, from ~ 0.15 at $B = 0.016H_{c2}$ to ~ 0.23 at $B = 0.1H_{c2}$. At the lowest field, $B = 0.016H_{c2}$, the maximum current is $J_c \approx 0.0383J_0$ corresponding to 10% of the depairing current. The movie in [39] demonstrates the evolution of vortex dynamics with increasing particle density for this magnetic field.

Figure 1(c) presents the dependences of the critical currents J_c on the nonsuperconducting volume fraction f for different particle diameters at $B = 0.1H_{c2}$. The highest critical current is realized at $a = 3\xi$ indicating the existence of an optimal particle size. By applying parabolic fits to the numerical data for the geometry dependent $J_c(a, f)$, we found the optimal particle size and volume fraction at several fields. Figure 2(a) shows the magnetic field dependences of the optimal particle size a_{opt} and volume fraction f_{opt} in the range $0.016H_{c2} < B < 0.2H_{c2}$. Within this range the optimal size monotonically decreases with the increasing magnetic field from $\sim 4.5\xi$ to $\sim 2.5\xi$. This indicates that the typical scale of disorder has to be comparable with the intervortex spacing which decreases as $1/\sqrt{B}$. The optimal volume fraction has a weak, non-monotonic dependence on the field strength, but stays within the range of 17–22%. The magnetic-field dependence of the maximum critical current achieved for the optimal parameters is shown in Fig. 2(b).

To characterize the structure of the pinned vortex

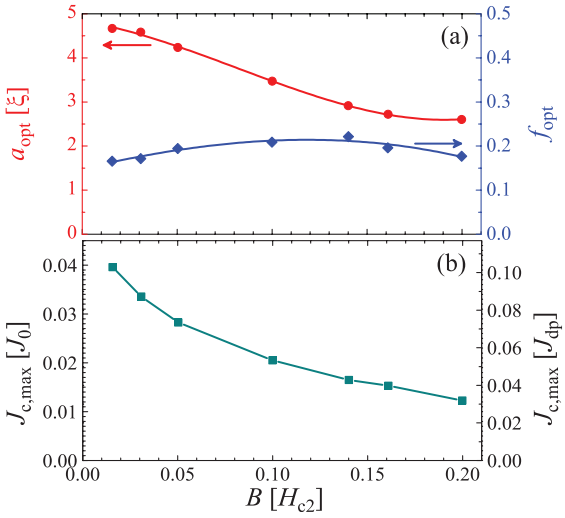

Figure 2. (a) The magnetic field dependence of the optimal diameter (left axis) and volume fraction (right axis). (b) The maximum critical current for optimal parameters for different magnetic fields in reduced units. The right axis shows this current normalized to the depairing current.

states, we extracted the field-induced vortex lines from the order parameter [40] and performed a detailed analysis of these configurations. We analyzed trapped vortex configurations at the final currents of the simulation sequences which are below the corresponding critical currents. Figure 1(d) shows a representative configuration for $B = 0.016H_{c2}$ imaged by the order-parameter isosurfaces $|\psi(\mathbf{r})| = 0.1$. Both particles and vortex lines can be seen as regions of suppressed order parameter. We found that the vortex arrangements typically are quite disordered, which is partly caused by the interaction of the vortices with randomly arranged particles and partly by incomplete equilibration. Vortex lines traced from this order-parameter distribution are shown in Fig. 1(e). They are split into line segments located inside the particles and in superconducting material, as illustrated by blue and red lines, respectively.

We extracted several parameters characterizing trapped configurations: (i) The fraction of particles occupied by vortices, f_{fill}, (ii) the fraction of particles double-occupied by vortices, f_2, (iii) the fraction of the total line length located outside particles, $f_{free} = \ell_{outside}/\ell_{total}$, (iv) the average length of line segments trapped between neighboring particles, L_t, see inset in Fig. 3(c), and (v) the average particle-to-particle displacement in the direction of motion, $u_l = u_y$, and in transverse direction $u_t = u_x$. These parameters are not independent. Indeed, the number of particles holding a given vortex line can be estimated as $f_{free}L_z/L_t$ meaning that the total number of occupied pins is $N_v f_{free}L_z/L_t$, where N_v is the total number of vortex lines. As fraction of pins f_2 is holding two vortex lines, we can estimate the occupied fraction as $f_{fill} \approx N_v f_{free}L_z/[N_p(1 + f_2)L_t]$. We checked that the

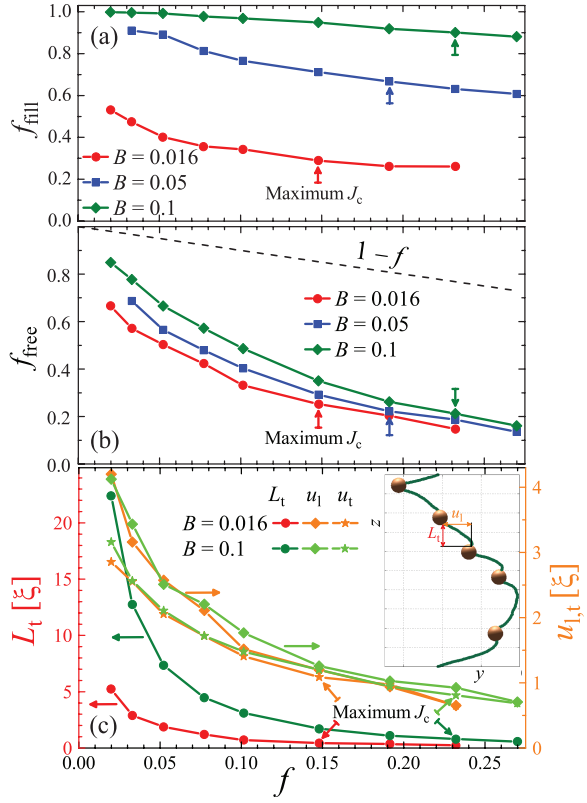

Figure 3. Evolution of parameters characterizing pinned vortex-line configurations with increasing nonsuperconducting volume fraction f for $a = 4\xi$ and three magnetic fields. The plot (a) shows the fraction of particles occupied by vortex lines, $f_{\rm fill}$. The plot (b) presents the length fraction of vortex segments outside the particles, $f_{\rm free}$. Dashed line shows the volume fraction occupied by superconducting material, $1-f$. The plot (c) shows the average geometrical parameters characterizing pinned line segments as illustrated in the inset, the segment length $L_{\rm t}$ (left axis) and typical pin-to-pin line displacements in the direction of motion, $u_{\rm l}$, and in the transverse direction, $u_{\rm t}$ (right axis). The parameters $L_{\rm t}$ and $u_{\rm l}$ are defined in the inset. In all plots arrows mark locations of the maximum critical current.

extracted parameters satisfy this consistency condition.

Particle fraction occupied by the vortex lines, $f_{\rm fill}$, naturally characterizes the efficiency of pin utilization. Figure 3(a) shows the dependence of this parameter on the nonsuperconducting volume fraction f for $a = 4\xi$ and three magnetic fields. As expected, this parameter increases with the magnetic field and decreases with the number of particles. For $B = 0.1H_{\rm c2}$ almost all particles are occupied. We also found that for this field typically 3–5% of particles hold two vortex lines without any systematic dependence on the particle density. For smaller fields the number of double-occupied particles is negligible. An noteworthy feature is that for small fields a significant fraction of particles remains unoccupied even for very low particle densities.

The efficiency of the vortex trapping by the particles can be characterized by the free-segment length fraction of the vortex lines, $f_{\rm free}$, plotted in Fig. 3(b). A natural upper limit for $f_{\rm free}$ is the volume fraction occupied by the superconducting material, $1-f$, shown by the dashed line. This limit would be realized if there were no correlations between particles and vortices. We can see that for pinned configurations $f_{\rm free}$ is significantly below this limit since particles trap vortices. Notably, $f_{\rm free}$ drops below 50% when particles occupy only 5% of the volume for $B = 0.016H_{\rm c2}$. The free-segment fraction monotonically increases with the magnetic field, because the vortex lines compete for the particles. We observe that the maximum critical current is realized for $f_{\rm free} = 21$–25% which only weakly depends on the magnetic field.

For strong pinning sites the vortex lines split into finite-size segments hanging in between neighboring sites [5, 6, 8]. Figure 3(c) shows the behavior of the average length parameters in units of ξ characterizing these free-line segments, the segment length $L_{\rm t}$ and pin-to-pin line displacements in the direction of motion, $u_{\rm l}$, and in the transverse direction, $u_{\rm t}$. The length $L_{\rm t}$ rapidly increases with decreasing particle density and with increasing magnetic field. While the displacements $u_{\rm l,t}$ also increase with decreasing f, they only weakly depend on the magnetic field. As expected, for small particle densities the vortices stretch between pinning sites preferentially in the direction of motion [5, 6, 8] meaning that u_l is larger than u_t. These parameters, however, become almost identical for $f \gtrsim 0.15$. At the particle density corresponding to the maximum of the critical current all three parameters, $L_{\rm t}$, $u_{\rm l}$, and $u_{\rm t}$, are close to ξ for both magnetic fields.

In summary, we conducted a systematic study of vortex pinning by randomly distributed metallic inclusions within the superconductor using large-scale numerical simulations. Using this approach enables us now to predict optimal parameters for highest critical currents. We also analyzed statistical properties of pinned vortex arrays and revealed several nontrivial structural properties of the optimally-pinned states. Our general observation is that there is no universal optimal pinning configuration for all magnetic fields. Thus, for best performance in a given application, pinning landscapes should be designed taking into account relevant magnetic fields.

The authors acknowledge fruitful discussions with W. K. Kwok, U. Welp, M. Leroux, V. B. Geshkenbein, and R. Willa. This work was supported by the Scientific Discovery through Advanced Computing (SciDAC) program funded by U.S. DOE, Office of Science, Advanced Scientific Computing Research and Basic Energy Science. A.E.K. was supported by the Center for Emergent Superconductivity, an Energy Frontier Research Center funded by the U.S. DOE, Office of Science, Office of Basic Energy Sciences. C.L.P. was funded by the Office of the Director through the Named Postdoctoral Fellowship Program (Aneesur Rahman Postdoctoral Fellowship), Argonne National Laboratory.

[1] G. Blatter, M. V. Feigelman, V. B. Geshkenbein, A. I. Larkin, and V. M. Vinokur, Rev. Mod. Phys. **66**, 1125 (1994).
[2] E. H. Brandt, Rep. Prog. Phys. **58**, 1465 (1995).
[3] G. Blatter and V. B. Geshkenbein, *in "The Physics of Superconductors", Vol 1: Conventional and High-T_c Superconductors*, edited by K. Bennemann and J. Ketterson (Springer, Berlin, 2003) p. 726.
[4] A. I. Larkin and Y. N. Ovchinnikov, J. Low Temp. Phys. **34**, 409 (1979).
[5] Y. N. Ovchinnikov and B. I. Ivlev, Phys. Rev. B **43**, 8024 (1991).
[6] G. Blatter, V. B. Geshkenbein, and J. A. G. Koopmann, Phys. Rev. Lett. **92**, 067009 (2004).
[7] D. Ertaş and M. Kardar, Phys. Rev. B **53**, 3520 (1996).
[8] A. E. Koshelev and A. B. Kolton, Phys. Rev. B **84**, 104528 (2011).
[9] A. van Otterlo, R. T. Scalettar, G. T. Zimányi, R. Olsson, A. Petrean, W. Kwok, and V. Vinokur, Phys. Rev. Lett. **84**, 2493 (2000).
[10] S. Bustingorry, L. F. Cugliandolo, and D. Domínguez, Phys. Rev. B **75**, 024506 (2007).
[11] M.-B. Luo and X. Hu, Phys. Rev. Lett. **98**, 267002 (2007).
[12] U. Dobramysl, H. Assi, M. Pleimling, and U. Täuber, Eur. Phys. J. B **86**, 228 (2013).
[13] J. L. MacManus-Driscoll, S. R. Foltyn, Q. X. Jia, H. Wang, A. Serquis, B. Maiorov, L. Civale, Y. Lin, M. E. Hawley, M. P. Maley, and D. E. Peterson, Appl. Phys. Lett. **84**, 5329 (2004).
[14] T. Haugan, P. N. Barnes, R. Wheeler, F. Meisenkothen, and M. Sumption, Nature **430**, 867 (2004).
[15] X. Song, Z. Chen, S.-I. Kim, D. M. Feldmann, D. Larbalestier, J. Reeves, Y. Xie, and V. Selvamanickam, Appl. Phys. Lett. **88**, 212508 (2006).
[16] J. Gutierrez, A. Llordes, J. Gazquez, M. Gibert, N. Roma, A. Pomar, F. Sandiumenge, N. Mestres, T. Puig, and X. Obradors, Nat. Mater. **6**, 367 (2007).
[17] H. Yamasaki, K. Ohki, H. Yamada, Y. Nakagawa, and Y. Mawatari, Supercond. Sci. Technol. **21**, 125011 (2008).
[18] Ö. Polat, J. W. Sinclair, Y. L. Zuev, J. R. Thompson, D. K. Christen, S. W. Cook, D. Kumar, Y. Chen, and V. Selvamanickam, Phys. Rev. B **84**, 024519 (2011).
[19] M. Miura, B. Maiorov, S. A. Baily, N. Haberkorn, J. O. Willis, K. Marken, T. Izumi, Y. Shiohara, and L. Civale, Phys. Rev. B **83**, 184519 (2011); M. Miura, B. Maiorov, J. O. Willis, T. Kato, M. Sato, T. Izumi, Y. Shiohara, and L. Civale, Supercond. Sci. Technol. **26**, 035008 (2013).
[20] A. Goyal, S. Kang, K. J. Leonard, P. M. Martin, A. A. Gapud, M. Varela, M. Paranthaman, A. O. Ijaduola, E. D. Specht, J. R. Thompson, D. K. Christen, S. J. Pennycook, and F. A. List, Supercond. Sci. Technol. **18**, 1533 (2005); S. Kang, A. Goyal, J. Li, A. A. Gapud, P. M. Martin, L. Heatherly, J. R. Thompson, D. K. Christen, F. A. List, M. Paranthaman, and D. F. Lee, Science **311**, 1911 (2006).
[21] B. Maiorov, S. A. Baily, H. Zhou, O. Ugurlu, J. A. Kennison, P. C. Dowden, T. G. Holesinger, S. R. Foltyn, and L. Civale, Nat. Mater. **8**, 398 (2009).
[22] A. Malozemoff, Annu. Rev. Mater. Res. **42**, 373 (2012).
[23] Y. Jia, M. LeRoux, D. J. Miller, J. G. Wen, W. K. Kwok, U. Welp, M. W. Rupich, X. Li, S. Sathyamurthy, S. Fleshler, A. P. Malozemoff, A. Kayani, O. Ayala-Valenzuela, and L. Civale, Appl. Phys. Lett. **103**, 122601 (2013).
[24] H. Matsui, T. Ootsuka, H. Ogiso, H. Yamasaki, M. Sohma, I. Yamaguchi, T. Kumagai, and T. Manabe, J. Appl. Phys. **117**, 043911 (2015).
[25] A. Schmid, Phys. Kondens. Materie **5**, 302 (1966).
[26] M. M. Doria, J. E. Gubernatis, and D. Rainer, Phys. Rev. B **41**, 6335 (1990).
[27] M. Machida and H. Kaburaki, Phys. Rev. Lett. **71**, 3206 (1993).
[28] G. W. Crabtree, G. K. Leaf, H. G. Kaper, V. M. Vinokur, A. E. Koshelev, D. W. Braun, D. M. Levine, W. K. Kwok, and J. A. Fendrich, Physica C **263**, 401 (1996); D. W. Braun, G. W. Crabtree, H. G. Kaper, A. E. Koshelev, G. K. Leaf, D. M. Levine, and V. M. Vinokur, Phys. Rev. Lett. **76**, 831 (1996); G. W. Crabtree, D. O. Gunter, H. G. Kaper, A. E. Koshelev, G. K. Leaf, and V. M. Vinokur, Phys. Rev. B **61**, 1446 (2000).
[29] I. Aranson, B. Y. Shapiro, and V. Vinokur, Phys. Rev. Lett. **76**, 142 (1996).
[30] V. A. Schweigert, F. M. Peeters, and P. S. Deo, Phys. Rev. Lett. **81**, 2783 (1998); B. J. Baelus and F. M. Peeters, Phys. Rev. B **65**, 104515 (2002).
[31] T. Winiecki and C. S. Adams, Phys. Rev. B **65**, 104517 (2002).
[32] G. R. Berdiyorov, M. V. Milošević, and F. M. Peeters, Phys. Rev. B **74**, 174512 (2006); G. Berdiyorov, K. Harrabi, F. Oktasendra, K. Gasmi, A. I. Mansour, J. P. Maneval, and F. M. Peeters, Phys. Rev. B **90**, 054506 (2014).
[33] D. Y. Vodolazov, Phys. Rev. B **88**, 014525 (2013).
[34] I. A. Sadovskyy, A. E. Koshelev, A. Glatz, V. Ortalan, M. W. Rupich, and M. Leroux, Phys. Rev. Applied **5**, 014011 (2016).
[35] I. A. Sadovskyy, A. E. Koshelev, C. L. Phillips, D. A. Karpeyev, and A. Glatz, J. Comp. Phys. **294**, 639 (2015).
[36] A. Gurevich, Ann. Rev. Cond. Matt. Phys. **5**, 35 (2014).
[37] In Ref. [35] a somewhat different normalization has been considered where $\epsilon(\mathbf{r})$ in the bulk was taken as $\epsilon = T_C/T - 1$ and unit of length was the zero-temperature coherence length ξ_0. It is straightforward to demonstrate that selection of $\epsilon = 1$ is equivalent to transition to new units in which lengths are normalized to the temperature-dependent coherence length $\xi(T) = \xi_0/\sqrt{T_C/T - 1}$.
[38] We verified that for such large system size (i) simulation with just one realization of disorder is already sufficient for a reasonable estimate of the critical current and (ii) finite-size effects are weak. Using the periodic boundary conditions in y directions allows us to avoid the effect of surface barriers and directly extract the bulk critical currents.
[39] Animation in supplemental materials [URL] illustrates evolution of vortex dynamics for $B = 0.016H_{C2}$ with increasing particle density.
[40] C. L. Phillips, T. Peterka, D. Karpeyev, and A. Glatz, Phys. Rev. E **91**, 023311 (2015).